Biosynthesis of β-d-glucan'gold nanoparticles, cytotoxicity and oxidative stress in mouse splenocytes

Luis Hernández-Adame, Carlos Angulo, Karen Delgado, Marion Schiavone, Mathieu Castex, Gabriela Palestino, Lourdes Betancourt-Mendiola, Martha Reyes-Becerril

PII: S0141-8130(19)32695-9
DOI: https://doi.org/10.1016/j.ijbiomac.2019.05.065
Reference: BIOMAC 12350

To appear in: *International Journal of Biological Macromolecules*

Received date: 11 April 2019
Revised date: 7 May 2019
Accepted date: 9 May 2019

Please cite this article as: L. Hernández-Adame, C. Angulo, K. Delgado, et al., Biosynthesis of β-d-glucan'gold nanoparticles, cytotoxicity and oxidative stress in mouse splenocytes, International Journal of Biological Macromolecules, https://doi.org/10.1016/j.ijbiomac.2019.05.065

Biosynthesis of β-D-glucan-gold nanoparticles, cytotoxicity and oxidative stress in mouse splenocytes

Luis Hernández-Adame[1,2], Carlos Angulo[1], Karen Delgado[1], Marion Schiavone[3], Mathieu Castex[4], Gabriela Palestino[5], Lourdes Betancourt-Mendiola[5], Martha Reyes-Becerril[1]*

[1]Immunology & Vaccinology Group. Centro de Investigaciones Biológicas del Noroeste (CIBNOR), Av. Instituto Politécnico Nacional 195, Playa Palo de Santa Rita Sur, La Paz B.C.S. 23096, México

[2]CONACYT-Centro de Investigaciones Biológicas del Noroeste (CIBNOR), Instituto Politécnico Nacional 195, Playa Palo de Santa Rita Sur, La Paz, B.C.S, 23090, México.

[3]Laboratoire d'Ingénierie des Systèmes Biologiques et Procédés, Institut National des Sciences Appliquées de Toulouse, UPS, INP, Université de Toulouse, Toulouse, France.

[4]Lallemand SAS, Blagnac, France.

[5]Sección de Biotecnología, Centro de Investigación en Ciencias de la Salud y Biomedicina, Universidad Autónoma de San Luis Potosí, Av. Sierra Leona 550, Lomas 2ª. Sección, San Luis Potosí, 78210, México

*Corresponding author: mreyes04@cibnor.mx (M. Reyes-Becerril); Tel: +52 612 12 3 84 84

Abstract

This study reports biosynthesis of gold-nanoparticles (AuNPs) by using β-D-glucans isolated from the yeast *Yarrowia lypolitica* D1. β-D-glucans serve as reducing and stabilizing mediators that induce the formation of AuNPs on the outer surface of the own β-D-glucan. The systems were physicochemically characterized by ultraviolet visible (UV-Vis) spectroscopy, high-resolution transmission electron microscopy (HR-TEM), scanning electron microscope (SEM), energy-dispersive X-ray spectroscopy (EDS), and dynamic light scattering (DLS) analyses. The results revealed the generation of AuNPs with quasi-spherical shape or large one dimension (1D) gold-nanostructures (AuNSs) depending on the $HAuCl_4$ concentration. A cytotoxic study was assessed in mouse splenocytes. Contrary to that expected, important cytotoxicity was found in all β-D-gluc+AuNPs systems by oxidative stress increase. This study discusses the cytotoxic mechanism, suggesting that the resulting β-D-gluc+AuNPs systems may not be candidates for the formulation of immunostimulants or nanocarriers for biomedical applications.

Keywords: *Green biosynthesis; toxicity; immune system; mouse splenocytes; delivery vehicles.*

1. Introduction

Recently, the use of gold nanoparticles (AuNPs) has risen exponentially in the biomedical field [1]. Their uses have been suitable for applications in controlled drug and gene delivery [2], cancer treatment [3], biomedical imaging [4], photothermal therapy [5], as immunostimulatory agent [6], and many others [7,8]. Apart from all the positive aspects associated with their use, the physicochemical and biological effects that trigger cytotoxicity remain as one of the major research issues [9]. To date, several research studies have provided evidence that concentration, particle size, shape, and surface charge of the AuNPs are the main factors that influence the degree of cytotoxicity and bioaccumulation [10–13]. Once AuNPs enter into the body, they are exposed to biological molecules and proteins that are easily adsorbed onto the nanoparticle surface reducing its surface-free energy and leading to several cellular responses, including oxidation stress, inflammatory processes, and cell apoptosis [14,15].

As a strategy to reduce cytotoxicity and environmental impact of the AuNPs, its production is gaining attention through green chemistry methods by using extracts of living organisms [16,17]. One of them is biosynthesis with carbohydrates, such as β-D-glucans that might be used as reducing and stabilizing agents with a promising approach for biomedical applications [18–20]. β-D-glucans are a group of glucose polysaccharides found in plants, yeast, fungi, and some bacteria, which consist of linear β (1→3)-linked backbones with β (1→6)-linked side chains with different length and molecular weight, which usually form tertiary structures stabilized by interchain hydrogen bonds [21]. This group possesses high biological activity and is commonly used as stimulants of immune cells against cancer and pathogen infections [22]. Currently, the Food and Drug Administration (FDA) has approved several β-D-glucan-based products with health and food applications [23]. Despite of these positive attributes, few reports that describe the synthesis of AuNPs by using β-D-glucans (β-D-gluc+AuNPs) are available

[24,25]. This process can be possibly due to the high amount of hydroxyl (-OH) groups exposed on the β-D-glucan surface. This property can open a promising alternative to produce β-D-gluc+AuNPs composites with myriad applications in health and food manufacture [26–29]. Moreover, due to their nature and chemical composition, the β-D-gluc+AuNPs should be nontoxic and safe composites; nonetheless, their biosafety has not been demonstrated, which is critical because the combination of β-D-glucan with therapeutic molecules has demonstrated, in some cases, toxic effects in the mouse model [30,31]. Furthermore, yeast-derived β-D-glucans have never been studied for AuNPs synthesis and their biological effects examined. In this sense, this study reports biosynthesis, characterization and toxicological evaluation of β-D-gluc+AuNPs composites, surprisingly, demonstrating the cytotoxic effect and radical oxygen production in mouse leukocytes. This information establishes a precedent in this field, and together with complementary toxicological and biological studies, it may contribute to considerations for the development of new nanomedicines.

2. Materials and methods

2.1 General analysis of β-D-glucan D1

Yarrowia lipolytica strain D1 was used in this experiment [32] and glucan extraction was carried out according to Williams et al. [33]. The polysaccharide composition was measured by nuclear magnetic resonance (NMR). β-D-glucan D1 molecular weight was determined by Size Exclusion Chromatography - Multi Angle Light Scattering (SEC-MALS, Wyatt, Santa Barbara, CA) with a guard column (Shodex OHPAK SB804 HQ + SB 803HQ in series, Shodex, Tokio, JP). β-glucan Molecular Weight Standards (P-MWBGS, Megazyme Inc., Chicago, USA) from 650,000 g/mol to 35,600 g/mol were used to calibrate the method. The results were expressed in

a graphic form to be able to judge chromatography quality. The total carbohydrate content was detected using an established protocol [32].

2.2. Preparation of β-D-glucan stock

In a 250-mL flat bottom flask, an aqueous- β-D-glucan stock was prepared dissolving 100 mg of isolated β-D-glucans in 100 mL of ultra-purified Mili-Q water. Then, the flask was completely sealed, and the stock was heated in a temperature-controlled glycerin bath at 140 °C for four hours to break the intra- and intermolecular hydrogen bonds that support the β-D-glucan structure. A white-turbid solution was obtained in this reaction and immediately used in the next experiments.

2.3. Green synthesis of β-D-glucan-gold nanoparticles (β-D-gluc+AuNPs)

The freshly prepared β-D-glucan solution, chloroauric acid ($HAuCl_4$; 99.9%, Sigma Aldrich, St. Louis, Mo, USA) and sterilized ultra-purified Mili-Q water were used throughout all the process. In a typical synthesis, 17.85 mL of the freshly prepared β-D-glucan stock (1mg/mL) were heated at 90 °C under vigorous stirring for 15 min; then, 2.16 mL of a $HAuCl_4$ solution (2.94 mM) were added. The mixture was kept under stirring at 90 ºC for three hours and finally left to cool down naturally at room temperature. During reaction time, the solution turned to violet color, indicating the reduction of Au^{3+} ions to AuNPs. Finally, the samples were washed by centrifugation (4000 rpm, five min) removing the supernatant; the cleansing process was repeated two times re-suspending the samples in sterilized ultra-purified Mili-Q water with an ultrasonic bath and then storing at 4 °C until further experiments. Moreover, a set of β-D-gluc+AuNPs composites with a fixed concentration of 1mg/mL of β-D-glucans but two different gold contents were synthesized to analyze the influence on the particle morphology and its

toxicity. The samples were labeled as β-D-gluc+AuNP10 and β-D-gluc+AuNP50, which corresponded to gold loading of 10 and 50 nM, respectively.

2.4. Synthesis of gold nanoparticles (AuNPs) by Turkevich method

Citrate-stabilized AuNPs were prepared according to a modified Turkevich method [33]. Briefly, a 15-mL aqueous solution was warmed at 90 °C in a round bottom bottle. Then 2.16 mL of a $HAuCl_4$ solution (2.94 mM) was added. The new solution was stirred for five minutes by a magnetic bar and sealed with a rubber cap to prevent temperature gradients in the liquid. After that, a 4-mL citrate solution (1 mM) was added, and the reaction was carried out for 60 min of maturation time. During this time, the solution turned to light-violet color, indicating the reduction of the Au^{3+} ions to AuNPs. Finally, the solution was cooled naturally at room temperature.

2.5.Characterization

Shape and size distribution were determined by transmission electron microscopy (TEM) using a JEOL JEM-2100 operated at 200 kV. Also, the TEM was equipped with an energy-dispersive X-ray spectroscopy (EDS) accessory (INCA 2000, Oxford Instrument, UK) for the elemental and chemical analyses. The ζ-potential and hydrodynamic radius was determined by dynamic light scattering using a Nano Zetasizer (Malvern Panalytical Ltd, Malvern, UK). The sample preparation was performed by using the colloidal vibration method as reported previously [34].

2.6. Leukocytes isolation and experimental design

Healthy six adult male Cd/1 mice (10-12 week-old, 30 ± 5.0 g) were obtained from the Biotherium of Centro de Investigaciones Biologicas del Noroeste (CIBNOR), La Paz, BCS, Mexico. Murine spleen was obtained in accordance with the relevant guidelines and based on a previously described methodology [35]. Splenocytes were adjusted to 1.2 x 10^6 cells mL^{-1} with RPMI-1640 (GIBCO, Thermo Scientific, Waltham, MA, USA) plus 10% fetal bovine serum (GIBCO, Thermo Scientific, Waltham, MA, USA).

Eight hundred microliters of splenocytes (1.2 x 10^6 cells mL^{-1}) were dispensed into a 24-well flat-bottomed plate (Nunc Thermo Scientific, Waltham, MA, USA). Next, splenocytes were stimulated with 100 µL of β-D-glucans (200 µg mL^{-1}), β-D-gluc+AuNP10 (100 µg mL^{-1}+10 nM), β-D-gluc+AuNP50 (100 µg mL^{-1}+50 nM), AuNP10 (10 nM), and AuNP50 (50 nM) (obtaining a final concentration of leukocytes 1.0 x 10^6 cells mL^{-1} per well). Splenocytes were incubated at 37 °C (85% relative humidity 5% CO_2) for 24 h. Medium without experimental treatment was used as a control. Twenty four hours later, splenocytes were dispensed into 96-well microtitre plates (Nunc Thermo Scientific, Waltham, MA, USA) or placed in 5-mL tubes (Falcon, Becton Dickinson) for immunological or flow cytometry analysis. For gene expression, splenocytes were prepared according to our previous report [21].

2.7. Cell viability

Cell viability was measured by resazurin assay in splenocytes (1.0 x 10^6 cell mL) according to Riss et al. [36]. Splenocytes without any treatment and incubated with DMSO (Sigma, St. Louis, MO, USA) and RPMI alone plus treatments were used as controls. Twenty-four hours later, cells were marked with 10 µl resazurin solution (Sigma, St. Louis, MO, USA) at 37 °C (5% CO_2) for four hours.

Fluorescence intensity was detected at 590 nm excitation and 535 nm emission. Viability (%) was estimated as follows:

% viability = A sample/A negative control x 100

2.8. Immunological parameters

Before using flow cytometry for phagocytosis activity and oxidative stress (DHR 123), stimulated splenocytes were carefully filtered using a cell strainer with a mesh size of 40 mm (BD Bioscience, NJ, USA).

2.8.1. Phagocytic assay in immunostimulated splenocytes

The phagocytosis of splenocytes stimulated with β-D-glucans, AuNP10, AuNP50, β-D-gluc+AuNP10 and β-D-gluc+AuNP50 were studied using labeling *Saccharomyces cerevisiae* with fluorescein isothiocyanate (FITC) by flow cytometry at 24 h [35,37].

2.8.2. Respiratory burst activity

Reactive oxygen species activity was analyzed in immunostimulated splenocytes using dichlorofluorescein diacetate (DCF-DA) (Molecular Probes, Sigma, St. Louis, MO, USA) [38]. Briefly, splenocytes were incubated DCF-DA (16 μM) and re-suspended in RPMI for 30 min. Fluorescence was detected at 485 nm (excitation) and 520 nm (emission).

2.8.3. Nitric oxide (NO) production

Nitric oxide production was measured using Griess reagent (Sigma, St. Louis, MO, USA) [39]. One hundred of splenocytes (1.0 x 10^6 cell mL) was conjugated in one hundred of Griess solution and incubated at 25 °C in the dark for 15 min. Absorbance was read at 540 nm.

2.8.4. Peroxidase activity

Total peroxidase (PO) activity in splenocytes was assayed following the methodology of Quade and Roth [40]. Twenty microliters of splenocytes were incubated with 100 µL of 3,3´,5, 5´-tetramethylbenzidine hydrochloride (TMB, Genei Laboratories Pvt Ltd, Bangalore, India) (20 mM) and 10 µL of H_2O_2 (5 mM). The color change reaction (blue) was stopped with 50 µL of 4 M sulfuric acid (H_2SO_4) and read at 450 nm.

2.9. Antioxidant enzymes

2.9.1. Superoxide dismutase activity (SOD)

SOD activity was measured in splenocytes following the manufacturer's instructions and using a commercial kit of SOD (Cat. 19160, Sigma, St. Louis, MO, USA). The absorbance was determined at 440 nm.

2.9.2. Catalase activity (CAT)

Catalase activity was assayed according to Greenwald [41]. Briefly, fifty microliters of splenocytes were incubated with 25 µL assay buffer (100 mM potassium phosphate buffer, pH 7), 50 µL methanol (Sigma) and 5 µL hydrogen peroxide (Applichem, 30%) under continuous shaking at room temperature for 20 min. Then, 25 µL potassium hydroxide (10 M; Applichem, Chicago, USA) and 50 µL Purpald (46 mM in 0.5 M HCl; Sigma, St. Louis, MO, USA) were added and incubated at the same conditions. Finally, 25 µL potassium periodate (192 mM in 0.5 M potassium hydroxide) was added and incubated for five minutes and read at 540 nm.

2.10. Gene transcriptional analysis

2.10.1. Cytokines

The expression of cytokine genes (Table 1) in immunostimulated splenocytes was quantified using Real-Time PCR. The relative expression was calculated by the 2^{-DDCT} method, and gene transcription was calculated based on the expression of the elongation factor 1-alpha gene [42].

2.11. Scanning electron microscopy (SEM)

One milliliter of splenocytes stimulated with different treatments were collected at 24 h by centrifugation (1500 rpm, 4 °C, five min), the pellet was recovered and suspended in 100 μL of 2.5% glutaraldehyde in phosphate buffer saline (PBS, pH 7.4) at room temperature for 30 min. After rinsing, splenocytes were fixed in Os04 (1% in PBS, 4OC, 12 h) and rinsed twice. Splenocytes were dehydrated in a gradient acetone concentration (30% 50% 75% 90%, three times 100%). After dehydration, the resulting mixture was transferred to coverslips and left to dry at 25 °C for 24 h. Coverslips were mounted on aluminum stubs and examined in a scanning electron microscope Hitachi, S300N (Hitachi High-Technologies Co., Fukuoka, JP).

2.12. Statistical analysis

SPSS v.19.0 software (SPSS, Richmond, VA, USA) was used and one-way analysis of variance (ANOVA) and Tukey's multiple range test were performed to determine differences between treatments ($p < 0.05$).

3. Results

3.1. General analysis of β-D-glucan D1

The results of molecular weight and NMR analysis of β-D-glucans D1 are shown in Fig. 1, which displays that β-D-glucan D1 had a defining peak of 952 kDa (the mean of molecular weight of the distribution comprising the individual weight of every fraction). The ^{1}H-13^{C}

analysis confirmed the glycosidic arrangement and branch of the β-D-glucan (Fig 1b). Fig. 1b shows the typical signal characteristics of a β-D-glucan. The expanded spectral region from 4.29 - 453 ppm exhibits resonances with several inflection points for the anomeric proton, implying a (1/3)-β-D-glucan and demonstrating the existence of β-D-glucans obtained from *Y. lipolytica*. The goal of this study was to provide these insights of the polysaccharide structure using NMR; additionally, the examination showed that β-D-glucan D1 was found linear. The β-D-glucan D1 had 92% and 94% of purity for one and four hours, respectively, using the method of phenol-sulfuric acid.

3.2. Characterization of β-D-gluc+AuNPs

3.2.1. Optical and morphological characterization of β-D-glucans and β-D-gluc+AuNPs systems

The optical absorptions of β-D-glucans D1, AuNPs and β-D-gluc+AuNPs (see Fig. 2) consist of absorption in the visible region due to β-D-glucans with a main peak from 450 to 620 nm attributed to the surface plasmon resonance (SPR) derived from AuNPs, corresponding to pink and violet colors of each sample (see inset Fig 2). The AuNPs has a SPR strongly associated with the nanoparticle size, shape, and environment. In this sense, the most defined peak corresponded to AuNPs reduced by citrate. These particles were synthesized by the Turkevic method that has demonstrated to produce stable and homogeneous AuNPs [33]. The peak was centered at 542 nm and indicated the generation of quasi-spherical shape and small size distribution (29.6 ± 3.5 nm) of AuNPs as confirmed by the TEM image of Fig 3b and S1a, respectively. Likewise, the SPR corresponding to β-D-gluc+AuNPs systems showed important changes in their peak width, intensity and position. The most notable changes were observed for the sample β-D-gluc+AuNP10 that showed a broader SPR peak with a reduced intensity, denoting a wide NP size distribution with a variety of shapes and obviously a lower gold

concentration. These characteristics were confirmed by TEM images (see Fig. 3c), which showed AuNPs synthesized on the wall of the 1D hollow cavity of the β-D-glucan helical strands with a diameter of 45.8 ± 4.3 nm size and large 1D gold nanostructures (AuNSs) with lengths ranging from 200 to 1000 nm as shown in Fig. 3c and S1b, respectively. Additionally, the EDS mapping analysis in Fig. S2a confirmed the metallic gold composition of these 1D AuNSs, suggesting the reduction of the Au^{3+} ions to metallic nanostructures as a possible formation mechanism by the OH^- radicals exposed on the wall of the β-D-glucans, which will be discussed in the next section.

A rise in the concentration of $HAuCl_4$ during synthesis produces individual and well-dispersed AuNPs on the outer wall of β-D-glucans. It was confirmed in the β-D-gluc+AuNP50 sample that showed the SPR peak centered at 533 nm (Fig. 2), which corresponded to well dispersed AuNPs with quasi-spherical shape and 18.6 ± 5.5 nm in size distribution as demonstrated in the TEM image of Fig. 3d and S1c, respectively. Additionally, the EDS analysis of Fig. S2b confirmed the metallic nature of the AuNPs free of impurities.

3.2.2. Surface charge and hydrodynamic radius by Dynamic Light Scattering

Table II shows ζ- potential (ZP) by dynamic light scattering (DLS) measurements of all samples that revealed an interesting behavior in surface charge of β-D-glucans and β-D-gluc+AuNPs. As expected, the AuNPs reduced by citrate showed a negative ZP induced by the citrate ions anchored on the NP surface. Likewise, due to the large amount of OH groups forming the wall of some polysacchacarides, such as β-D-glucans, a cationic behavior was observed in all samples with the presence of β-D-glucans. The most positive value was recorded for water soluble β-D-glucans followed by β-D-gluc+AuNP10 that contained the lowest amount of gold (10 nM) and formed the 1D AuNSs. The β-D-gluc+AuNP50 (50 nM) showed a ZP of -

1.01 ± 0.2 mV when compared with the β-D-gluc+AuNP10 system; a change was observed on the particle surface, which indicated a decrease in the OH groups due to the reduction of Au(III) ions during formation of well-dispersed quasi-spherical gold nanoparticles on the outer wall of β-D-glucans. The hydrodynamic radius for all systems was also determined by DLS and summarized in Table II, which confirmed the narrow size distribution of the AuNPs reduced by citrate and the large structures in the micrometer range for the β-D-glucans and β-D-gluc+AuNPs systems.

3.2.3. Formation mechanism of β-D-gluc+AuNPs systems

According to the foregoing results, the following mechanism for the formation of the AuNPs and the AuNSs on the wall of β-D-glucans was proposed; as a first step, the $Au(OH)_4^-$ ions solubilized in the aqueous solution at boiling point were attracted on the walls of β-D-glucans by electrostatic interactions due to the cationic nature of this polysaccharide. Temperate and reactivity nature of the OH groups used as electron source started the redox reactions to form the gold nuclei at the beginning of the reaction followed by a constant attraction, reducing the Au(III) ions to generate the AuNPs [25]. In the case of the ID AuNSs, during the nucleus stage, the ratio between OH groups and Au(III) ions was so large that it must have induced an increasing amount of gold nuclei on the wall of β-D-glucans. Also, the remnant Au(III) ions adsorbed on the nuclei and the wall of β-D-glucan promoted the van der Waals attractive interactions between the nuclei until they collapsed and reached a self-assemblage in the 1D AuNSs.

3.3. In vitro experiment using splenocytes

3.3.1. Viability

The viability of splenocytes was higher 80% after stimulation with β-D-glucans, AuNP10 and AuNP50 treatments (Fig. 4). By contrast, the combination of β-D-gluc+AuNP10 and β-D-gluc+AuNP50 dramatically reduced the viability of splenocytes (< 45%) causing cytotoxicity of splenocytes. The DMSO positive control of cytotoxicity reduced the cell viability to 10%.

3.3.2. Immunological and antioxidant responses

Splenocytes stimulated with AuNP10 and AuNP50 significantly increased phagocytic ability (non-stimulated leukocytes) (Fig. 5a) followed by β-D-glucans or the control group. In contrast, the combination of β-D-gluc+AuNP10 or β-D-gluc+AuNP50 decreased phagocytic activity in the stimulated splenocytes.

Splenocytes exposed to β-D-gluc+AuNP10 or β-D-gluc+AuNP50 produced an increase in ROS production measured by the emitted fluorescence of DCFH-DA (Fig. 5b), which was associated with the phagocytosis activity.

In this study, nitric oxide production increased ($P < 0.05$) in splenocytes incubated with β-D-glucans, β-D-gluc+AuNP10 or β-D-gluc+AuNP50 respect to control splenocytes (Fig.6a).

Interestingly, a lower ($P < 0.05$) peroxidase activity could be observed after stimulation with any treatments in comparison with the control group (Fig 6b).

Regarding antioxidant enzymes, superoxide dismutase activity was similar among treatments and the control group (Fig.7a). However, with respect to the control cells, catalase activity significantly augmented in splenocytes incubated with β-D-glucans, β-D-gluc+AuNP10 or β-D-gluc+AuNP50 treatments at 24 h (Fig. 7b).

3.3.3. Cytokine gene expression levels

Figure 8 describes immune related-gene expression of splenocytes following incubation with β-D-glucans, β-D-gluc+AuNP10 or β-D-gluc+AuNP50 for 24 h. Firstly, dectin-1 gene up-regulated after β-D-glucan stimulation followed by β-D-gluc+AuNP10 and β-D-gluc+AuNP50 with respect to the control group or AuNPs treatments. The NF-κβ, IL-1β, and TNF-α gene transcription levels significantly increased in splenocytes incubated with β-D-glucans treatment followed by β-D-gluc+AuNP10.

3.3.4. Splenocytes interaction with β-D-glucans, β-D-gluc+AuNP10-50 and AuNP10-50 by SEM

After 24 h, splenocytes exposed to different treatments were analyzed by SEM (Fig. 9). The ultrastructural features revealed the interaction of β-D-glucans, β-D-gluc+AuNP10-50 and AuNP10-50 with mouse splenocytes. Control cells without particles were normal (Fig. 9a). Apparently, β-D-glucans, AuNP10 and AuNP50 treatments did not modify cellular uptake (Fig. 9ce). Interestingly, splenocytes exposed to combined treatments (e.g. β-D-gluc+AuNP10 or β-D-gluc+AuNP50) showed distinguishable characteristics of apoptosis, such as holes, separated apoptotic bodies and morphological alteration in a larger proportion of cells (Fig. 9de).

4. Discussion

Macromolecule-stabilized nanoparticles are particularly interesting due to their excellent biocompatibility and potential biological activities. Among the most used nanoparticles, AuNPs have been extensively used in a wide variety of technological applications, such as catalysis, organic photovoltaics, electronic design, water and environmental remediation, sensory probes, and drug delivery [7]. The most common synthesis of AuNPs is a redox reaction of Au(III) ions by citrate; however, in the increasing search for developing smart or advanced materials, several coatings have been tested to stabilize the AuNPs surface and reduce the agglomerates and

aggregates [43]. The aggregation of the AuNPs can be avoided by modifying their surface with biocompatible ligands and/or polymers, which are anchored on the NPs surface by chemical or physical adsorption [29]. These surface changes can also improve hydrophilicity, and in some cases, direct the AuNPs to specific cells. Recently, some reports have shown that the use of delivery vehicles, such as chitosan, alginate, and among other carriers, could enhance the activity of immunostimulants [44]. In this sense, β-D-glucan with high immunostimulant properties may open a new field in the development of delivery vehicles [31]. This study used β-D-glucans isolated from the yeast *Yarrowia lipolytica* D1, proving their capacity to reduce Au(III) ions to metallic nanoparticles and assessing their biological interaction in mouse spleen leukocytes. β-D-glucan D1 characterization showed the typical signal of a β-D-glucan: glycosidic configuration and linkage by NMR, low molecular weight and purity [45]. Studies have suggested that immunomodulatory properties of β-D-glucans are associated with molecular weight. β-D-glucans with high molecular weight increase the production of proinflammatory cytokines while those with low molecular weight activate leukocytes via nuclear transcription factors [46]. Fungal-derived β-D-glucan showed that Dectin-1 mediated the production of the pro-inflammatory TNF-α gene in response to zymosan [49]. Additionally, this study proved that the chemical arrangement of the OH groups in this β-D-glucan have the capacity to produce 1D AuNSs. In literature, two reports have shown the ability of β-D-(1-3)-glucans derived from Curdlan [47] and *Lentinus edodes* [25] to produce 1D AuNSs. These β-D-glucans are very promising candidates to produce 1D nanostructures in biomedical and technological fields as immunostimulants. Once all systems (β-D-glucans, AuNPs, and β-D-gluc+AuNPs) were characterized, their possible application in nanomedicine was assessed using mouse splenocytes. Biosecurity and control of nanoparticles and macromolecules, such as β-D-glucans, are essential for the effective utilization of those resources before their application in an *in vivo* experiment in

biomedicine. The AuNPs or β-D-glucan tested in this study did not induce cell death; however, high toxicity was observed when they were combined, principally in splenocytes exposed to β-D-gluc+AuNP50 treatment. Gold nanoparticles are usually safe and several toxicity studies have evaluated that their LD50 is safe enough up to 1 mg/mL [48]. β-D-glucans have demonstrated an important immunostimulant effect protecting the immune system from bacterial, parasitic and viral infection [49]. In this study, β-D-glucan functionalized with gold nanoparticles showed concentration-dependent cytotoxicity. Contrary to our study, Pooja et al. [50] experimented with A549 human lung cancer cells exposed to blank xanthan stabilized gold nanoparticles and observed they were non-toxic and biocompatible at any test concentration. The chemical characteristics of gold nanoparticles, such as size, solubility and surface modification have been well studied. Scott and collaborators [51] studied the phagocytosis of gold nanoparticles and concluded that it is size dependent where the kinetics and saturation of endocytosed nanoparticles depend upon the physical dimensions [52] for example, gold nanoparticles where minimal sizes (< 2 nm) cause cytotoxicity within 12 h and nanoparticles > 15 nm in size are nontoxic. In this study, gold nanoparticles alone had 30 nm in size, and conjugated with β-D-glucan, they had about 45 nm in size; therefore, the size of the nano-complexes used should not cause cytotoxicity. Hauck et al. [53] evaluated the size and shape of nanoparticles and observed that these characteristics affect its uptake and removal by cells. For example, for hyperthermia-based cancer therapy the gold nanorods are promising candidates [54,55]. Curiously, in the experiment performed in this study, gold nanoparticles changed their sphered form to large 1D structures similar to nanorods when they were combined with β-D-glucan. *In vitro* studies with human cancer cell line exposed to gold nanorods showed more cytotoxicity than gold nanospheres [56,57]. This mortality might be shape-dependent; however, the exact mechanism and role of glucan present on gold nanoparticle require further exhaustive assessment. In

addition, other studies had no detect effects of NPs on the viability and morphological integrity of cells [58,59] as we have noticed in leukocytes exposed to AuNPs or β-D-glucan, which accounts for their biocompatibility.

Željka Krpetić et al. [60] demonstrated that gold particles are phagocytized by leukocytes via endocytosis. In this study, the phagocytosis assay was analyzed by flow cytometry and ROS production by DCF-DA. The phagocytosis activity was enhanced in splenocytes stimulated with AuNP10 or AuNP50 treatments and decreased significantly in splenocytes stimulated with the conjugate β-D-gluc+AuNP10 or β-D-gluc+AuNP50 compared with the control group; however these nano-complexes (β-D-gluc+AuNP10 or 50) increased the ROS production in a dose-dependent manner. This ROS generation could be reflected like a toxic damage [48]. In this manner, the cellular death observed in these complexes could be attributed to an increase in ROS production. Likewise, nitric oxide production and catalase activity were enhanced in these β-D-glucan+NPs treatments as in the β-D-glucan alone treatment. Nonetheless, these increases in splenocytes stimulated with β-D-glucan might be a positive immunostimulant response, and in those splenocytes treated with β-D-gluc+AuNPs, it could be a response caused by oxidative injury related to the cytotoxicity observed in the Resazurin assay. Nitric oxide is an important antimicrobial agent against bacterial or viral pathogens [61]. The term antioxidant refers to the chemical material that prevents the use of oxygen. Catalase enzyme is an agent that acts against the harmful effects of free radicals, such as hydrogen peroxide. Barath Manikanth et al. [62] evaluated the antioxidant function of gold nanoparticles and observed the inhibition of reactive oxygen species and scavenging free radicals. In this study, the increase in catalase activity after β-D-gluc+AuNPs (10 or 50 nM) treatments in splenocytes could be due to an increase in hydrogen peroxide in response to stress conditions. β-D-glucan may stimulate several pro-inflammatory cytokines and nitric oxide production by macrophages [63]. In the results of this

study, IL-1β and TNF-α, mRNA gene expression could be highly up-regulated after β-D-glucan stimulation in splenocytes and down-regulated in β-D-gluc+AuNP50 and AuNP10 or 50 treatments. Likewise, Shukla et al. [64] showed that bare gold nanoparticles are biocompatible, noncytotoxic and nonimmunogenic and do not generate reactive oxygen species production, and the cytokines, such as TNF-α and IL-1β, are down-regulated.

This study also evaluated the gene expression of dectin-1 and NF-κβ gene expression after stimuli with β-D-glucans, β-D-gluc+AuNP10-50 and AuNP10-50, where an important dectin-1 up-regulation was found after β-D-glucans treatment, including β-D-gluc+AuNP10-50. In general, an increase of dectin-1 transcription in splenocytes exposed to β-D-glucans treatments was expected because dectin-1 is the primary receptor on leukocytes that recognizes β-D-glucans inducing pro-inflammatory cytokines and transcription factors [65], as it was observed in this study after stimulation with β-D-glucans.

Finally, this study observed by SEM analysis that β-D-glucans or AuNP10-50 did not cause cellular toxicity. Unfortunately, conjugate β-D-gluc+AuNP10-50 treatments showed an interesting cytotoxicity generating a response to oxidative stress. Remaining questions arise to know the mechanism involved in the observed cytotoxicity that merit more studies.

Conclusion

The results of this study showed that AuNPs coupled with β-D-glucan caused an important cytotoxicity by an increase in oxidative stress while β-D-glucan or AuNPs alone did not. β-D-glucan alone could directly activate mouse spleen leukocytes, increasing their viability and antioxidant enzyme activities. In contrast, this study suggests that AuNPs coupled with β-D-glucan nanoparticle is not a candidate with possible uses in biomedical application.

Acknowledgments

The authors are thankful to Ariel Cruz for his help in SEM sessions, Amaury Cordero and Guadalupe Sanchez Castro for their kind help with mice CD1, and Diana Fischer for English edition of this article. This research was financed by CONACYT/Mexico: FC2016/2820, PDCPN2014/248033 and INFR2014/225924 projects.

Conflict of Interests

The authors declare that they have no conflict of interest for the publication of this article.

References

[1] Z. Miao, Z. Gao, R. Chen, X. Yu, Z. Su, G. Wei, Surface-bioengineered Gold Nanoparticles for Biomedical Applications, 25 (16) (2018) 1920-1944. doi:10.2174/0929867325666180117111404.

[2] P. Ghosh, G. Han, M. De, C.K. Kim, V.M. Rotello, Gold nanoparticles in delivery applications, Adv. Drug Deliv. Rev. 60 (2008) 1307–1315. doi:10.1016/j.addr.2008.03.016.

[3] A. Kumar, H. Ma, X. Zhang, K. Huang, S. Jin, J. Liu, T. Wei, W. Cao, G. Zou, X.-J. Liang, Gold nanoparticles functionalized with therapeutic and targeted peptides for cancer treatment, Biomaterials. 33 (2012) 1180–1189. doi:10.1016/j.biomaterials.2011.10.058.

[4] E. Hutter, D. Maysinger, Gold nanoparticles and quantum dots for bioimaging, Microsc. Res. Tech. 74 (2011) 592–604. doi:10.1002/jemt.20928.

[5] L.C. Kennedy, L.R. Bickford, N.A. Lewinski, A.J. Coughlin, Y. Hu, E.S. Day, J.L. West, R.A. Drezek, A New Era for Cancer Treatment: Gold-Nanoparticle-Mediated Thermal Therapies, Small. 7 (2011) 169–183. doi:10.1002/smll.201000134.

[6] M. Tello-Olea, S. Rosales-Mendoza, A.I. Campa-Córdova, G. Palestino, A. Luna-González, M. Reyes-Becerril, E. Velazquez, L. Hernandez-Adame, C. Angulo, Gold nanoparticles (AuNP) exert immunostimulatory and protective effects in shrimp (Litopenaeus vannamei) against Vibrio parahaemolyticus, Fish Shellfish Immunol. 84 (2019) 756–767. doi:10.1016/j.fsi.2018.10.056.

[7] A.F. Versiani, L.M. Andrade, E.M. Martins, S. Scalzo, J.M. Geraldo, C.R. Chaves, D.C. Ferreira, M. Ladeira, S. Guatimosim, L.O. Ladeira, F.G. da Fonseca, Gold nanoparticles and their applications in biomedicine, Future Virol. 11 (2016) 293–309. doi:10.2217/fvl-2015-0010.

[8] R.A. Sperling, P.R. Gil, F. Zhang, M. Zanella, W.J. Parak, Biological applications of gold nanoparticles, Chem. Soc. Rev. 37 (2008) 1896–1908. doi:10.1039/B712170A.

[9] P. Ganguly, A. Breen, S.C. Pillai, Toxicity of Nanomaterials: Exposure, Pathways, Assessment, and Recent Advances, ACS Biomater. Sci. Eng. 4 (2018) 2237–2275. doi:10.1021/acsbiomaterials.8b00068.

[10] C. Rambanapasi, J.R. Zeevaart, H. Buntting, C. Bester, D. Kotze, R. Hayeshi, A. Grobler, Bioaccumulation and Subchronic Toxicity of 14 nm Gold Nanoparticles in Rats, Molecules. 21 (2016) 763. doi:10.3390/molecules21060763.

[11] X. Li, Z. Hu, J. Ma, X. Wang, Y. Zhang, W. Wang, Z. Yuan, The systematic evaluation of size-dependent toxicity and multi-time biodistribution of gold nanoparticles, Colloids Surf. B Biointerfaces. 167 (2018) 260–266. doi:10.1016/j.colsurfb.2018.04.005.

[12] Y. Pan, S. Neuss, A. Leifert, M. Fischler, F. Wen, U. Simon, G. Schmid, W. Brandau, W. Jahnen-Dechent, Size-Dependent Cytotoxicity of Gold Nanoparticles, Small. 3 (2007) 1941–1949. doi:10.1002/smll.200700378.

[13] S.J. Soenen, B. Manshian, J.M. Montenegro, F. Amin, B. Meermann, T. Thiron, M. Cornelissen, F. Vanhaecke, S. Doak, W.J. Parak, S. De Smedt, K. Braeckmans, Cytotoxic Effects of Gold Nanoparticles: A Multiparametric Study, ACS Nano. 6 (2012) 5767–5783. doi:10.1021/nn301714n.

[14] P. Wang, X. Wang, L. Wang, X. Hou, W. Liu, C. Chen, Interaction of gold nanoparticles with proteins and cells, Sci. Technol. Adv. Mater. 16 (2015) 034610. doi:10.1088/1468-6996/16/3/034610.

[15] X. Liu, N. Huang, H. Li, Q. Jin, J. Ji, Surface and Size Effects on Cell Interaction of Gold Nanoparticles with Both Phagocytic and Nonphagocytic Cells, Langmuir. 29 (2013) 9138–9148. doi:10.1021/la401556k.

[16] C. Balalakshmi, K. Gopinath, M. Govindarajan, R. Lokesh, A. Arumugam, N.S. Alharbi, S. Kadaikunnan, J.M. Khaled, G. Benelli, Green synthesis of gold nanoparticles using a cheap Sphaeranthus indicus extract: Impact on plant cells and the aquatic crustacean Artemia nauplii, J. Photochem. Photobiol. B. 173 (2017) 598–605. doi:10.1016/j.jphotobiol.2017.06.040.

[17] M. Hamelian, K. Varmira, H. Veisi, Green synthesis and characterizations of gold nanoparticles using Thyme and survey cytotoxic effect, antibacterial and antioxidant potential, J. Photochem. Photobiol. B. 184 (2018) 71–79. doi:10.1016/j.jphotobiol.2018.05.016.

[18] P. Raveendran, J. Fu, S. L. Wallen, A simple and "green" method for the synthesis of Au, Ag, and Au–Ag alloy nanoparticles, Green Chem. 8 (2006) 34–38. doi:10.1039/B512540E.

[19] Poovathinthodiyil Raveendran, and Jie Fu, S.L. Wallen*, Completely "Green" Synthesis and Stabilization of Metal Nanoparticles, (2003). doi:10.1021/ja029267j.

[20] Y. Park, Y.N. Hong, A. Weyers, Y.S. Kim, R.J. Linhardt, Polysaccharides and phytochemicals: a natural reservoir for the green synthesis of gold and silver nanoparticles, IET Nanobiotechnol. 5 (2011) 69–78. doi:10.1049/iet-nbt.2010.0033.

[21] C. Velazquez-Carriles, M.E. Macias-Rodríguez, G.G. Carbajal-Arizaga, J. Silva-Jara, C. Angulo, M. Reyes-Becerril, Immobilizing yeast β-glucan on zinc-layered hydroxide nanoparticle improves innate immune response in fish leukocytes, Fish Shellfish Immunol. 82 (2018) 504–513. doi:10.1016/j.fsi.2018.08.055.

[22] M. Reyes-Becerril, F.A. Guardiola, V. Sanchez, M. Maldonado, C. Angulo, Sterigmatomyces halophilus β-glucan improves the immune response and bacterial resistance in Pacific red snapper (Lutjanus peru) peripheral blood leucocytes: In vitro study, Fish Shellfish Immunol. 78 (2018) 392–403. doi:10.1016/j.fsi.2018.04.043.

[23] D.J. Jenkins, C.W. Kendall, V. Vuksan, E. Vidgen, T. Parker, D. Faulkner, C.C. Mehling, M. Garsetti, G. Testolin, S.C. Cunnane, M.A. Ryan, P.N. Corey, Soluble fiber intake at a dose approved by the US Food and Drug Administration for a claim of health benefits: serum lipid risk factors for cardiovascular disease assessed in a randomized controlled crossover trial, Am. J. Clin. Nutr. 75 (2002) 834–839. doi:10.1093/ajcn/75.5.834.

[24] S. Anusuya, M. Sathiyabama, Preparation of β-d-glucan nanoparticles and its antifungal activity, Int. J. Biol. Macromol. 70 (2014) 440–443. doi:10.1016/j.ijbiomac.2014.07.011.

[25] X. Jia, X. Xu, L. Zhang, Synthesis and Stabilization of Gold Nanoparticles Induced by Denaturation and Renaturation of Triple Helical β-Glucan in Water, Biomacromolecules. 14 (2013) 1787–1794. doi:10.1021/bm400182q.

[26] I.K. Sen, K. Maity, S.S. Islam, Green synthesis of gold nanoparticles using a glucan of an edible mushroom and study of catalytic activity, Carbohydr. Polym. 91 (2013) 518–528. doi:10.1016/j.carbpol.2012.08.058.

[27] J.-K. Yan, J.-L. Liu, Y.-J. Sun, S. Tang, Z.-Y. Mo, Y.-S. Liu, Green synthesis of biocompatible carboxylic curdlan-capped gold nanoparticles and its interaction with protein, Carbohydr. Polym. 117 (2015) 771–777. doi:10.1016/j.carbpol.2014.10.048.

[28] W.-Y. Qiu, K. Wang, Y.-Y. Wang, Z.-C. Ding, L.-X. Wu, W.-D. Cai, J.-K. Yan, pH dependent green synthesis of gold nanoparticles by completely C6-carboxylated curdlan under high temperature and various pH conditions, Int. J. Biol. Macromol. 106 (2018) 498–506. doi:10.1016/j.ijbiomac.2017.08.029.

[29] Y. Meng, L. Cai, X. Xu, L. Zhang, Construction of size-controllable gold nanoparticles immobilized on polysaccharide nanotubes by in situ one-pot synthesis, Int. J. Biol. Macromol. 113 (2018) 240–247. doi:10.1016/j.ijbiomac.2018.02.122.

[30] H. Takahashi, N. Ohno, Y. Adachi, T. Yadomae, Association of immunological disorders in lethal side effect of NSAIDs on β-glucan-administered mice, FEMS Immunol. Med. Microbiol. 31 (2001) 1–14. doi:10.1111/j.1574-695X.2001.tb01579.x.

[31] S. Yoshioka, N. Ohno, T. Miura, Y. Adachi, T. Yadomae, Immunotoxicity of soluble β-glucans induced by indomethacin treatment, FEMS Immunol. Med. Microbiol. 21 (1998) 171–179. doi:10.1111/j.1574-695X.1998.tb01163.x.

[32] Michel. DuBois, K.A. Gilles, J.K. Hamilton, P.A. Rebers, Fred. Smith, Colorimetric Method for Determination of Sugars and Related Substances, Anal. Chem. 28 (1956) 350–356. doi:10.1021/ac60111a017.

[33] J. Turkevich, P.C. Stevenson, J. Hillier, A study of the nucleation and growth processes in the synthesis of colloidal gold, Discuss. Faraday Soc. 11 (1951) 55–75. doi:10.1039/DF9511100055.

[34] L. Hernandez-Adame, N. Cortez-Espinosa, D.P. Portales-Pérez, C. Castillo, W. Zhao, Z.N. Juarez, L.R. Hernandez, H. Bach, G. Palestino, Toxicity evaluation of high-fluorescent rare-earth metal nanoparticles for bioimaging applications, J. Biomed. Mater. Res. B Appl. Biomater. 105 (2017) 605–615. doi:10.1002/jbm.b.33577.

[35] M. Reyes-Becerril, F. Ascencio-Valle, I. Hirono, H. Kondo, W. Jirapongpairoj, M.A. Esteban, E. Alamillo, C. Angulo, TLR21's agonists in combination with Aeromonas antigens synergistically up-regulate functional TLR21 and cytokine gene expression in yellowtail leucocytes, Dev. Comp. Immunol. 61 (2016) 107–115. doi:10.1016/j.dci.2016.03.012.

[36] T.L. Riss, R.A. Moravec, A.L. Niles, S. Duellman, H.A. Benink, T.J. Worzella, L. Minor, Cell Viability Assays, in: G.S. Sittampalam, N.P. Coussens, K. Brimacombe, A. Grossman, M. Arkin, D. Auld, C. Austin, J. Baell, B. Bejcek, J.M.M. Caaveiro, T.D.Y. Chung, J.L. Dahlin, V. Devanaryan, T.L. Foley, M. Glicksman, M.D. Hall, J.V. Haas, J. Inglese, P.W. Iversen, S.D. Kahl, S.C. Kales, M. Lal-Nag, Z. Li, J. McGee, O. McManus, T. Riss, O.J. Trask, J.R. Weidner, M.J. Wildey, M. Xia, X. Xu (Eds.), Assay Guid. Man., Eli Lilly & Company and the National Center for Advancing Translational Sciences, Bethesda (MD), 2004. http://www.ncbi.nlm.nih.gov/books/NBK144065/ (accessed March 8, 2019).

[37] A. Rodríguez, M.Á. Esteban, J. Meseguer, Phagocytosis and peroxidase release by seabream (Sparus aurata L.) leucocytes in response to yeast cells, Anat. Rec. A. Discov. Mol. Cell. Evol. Biol. 272A (2003) 415–423. doi:10.1002/ar.a.10048.

[38] M. Ferreira-Cravo, F.R. Piedras, T.B. Moraes, J.L.R. Ferreira, D.P.S. de Freitas, M.D. Machado, L.A. Geracitano, J.M. Monserrat, Antioxidant responses and reactive oxygen species generation in different body regions of the estuarine polychaeta Laeonereis acuta (Nereididae), Chemosphere. 66 (2007) 1367–1374. doi:10.1016/j.chemosphere.2006.06.050.

[39] N.F. Neumann, D. Fagan, M. Belosevic, Macrophage activating factor(s) secreted by mitogen stimulated goldfish kidney leukocytes synergize with bacterial lipopolysaccharide to induce nitric

oxide production in teleost macrophages, Dev. Comp. Immunol. 19 (1995) 473–482. doi:10.1016/0145-305X(95)00032-O.
[40] M.J. Quade, J.A. Roth, A rapid, direct assay to measure degranulation of bovine neutrophil primary granules, Vet. Immunol. Immunopathol. 58 (1997) 239–248. doi:10.1016/S0165-2427(97)00048-2.
[41] R.A. Greenwald, Handbook Methods For Oxygen Radical Research, CRC Press, 2018. doi:10.1201/9781351072922.
[42] K.J. Livak, T.D. Schmittgen, Analysis of Relative Gene Expression Data Using Real-Time Quantitative PCR and the 2−ΔΔCT Method, Methods. 25 (2001) 402–408. doi:10.1006/meth.2001.1262.
[43] Y.-C. Yeh, B. Creran, V.M. Rotello, Gold Nanoparticles: Preparation, Properties, and Applications in Bionanotechnology, Nanoscale. 4 (2012) 1871–1880. doi:10.1039/c1nr11188d.
[44] J. Ji, D. Torrealba, À. Ruyra, N. Roher, Nanodelivery Systems as New Tools for Immunostimulant or Vaccine Administration: Targeting the Fish Immune System, Biology. 4 (2015) 664–696. doi:10.3390/biology4040664.
[45] P.A.J. Gorin, E. Barreto-bergter, 6 - The Chemistry of Polysaccharides of Fungi and Lichens, in: G.O. Aspinall (Ed.), The Polysaccharides, Academic Press, 1983: pp. 365–409. doi:10.1016/B978-0-12-065602-8.50011-X.
[46] G.D. Brown, J. Herre, D.L. Williams, J.A. Willment, A.S.J. Marshall, S. Gordon, Dectin-1 Mediates the Biological Effects of β-Glucans, J. Exp. Med. 197 (2003) 1119–1124. doi:10.1084/jem.20021890.
[47] K. Sugikawa, K. Kaneko, K. Sada, S. Shinkai, A Molecular Template Designed by the Modification of a Helix-Forming β-1,3-Glucan Polysaccharide To Fabricate One-Dimensional Nanostructures, Langmuir. 26 (2010) 19100–19105. doi:10.1021/la101335a.
[48] Z.P. Xu, Q.H. Zeng, G.Q. Lu, A.B. Yu, Inorganic nanoparticles as carriers for efficient cellular delivery, Chem. Eng. Sci. 61 (2006) 1027–1040. doi:10.1016/j.ces.2005.06.019.
[49] S. Rahar, G. Swami, N. Nagpal, M.A. Nagpal, G.S. Singh, Preparation, characterization, and biological properties of β-glucans, J. Adv. Pharm. Technol. Res. 2 (2011) 94. doi:10.4103/2231-4040.82953.
[50] D. Pooja, S. Panyaram, H. Kulhari, S.S. Rachamalla, R. Sistla, Xanthan gum stabilized gold nanoparticles: Characterization, biocompatibility, stability and cytotoxicity, Carbohydr. Polym. 110 (2014) 1–9. doi:10.1016/j.carbpol.2014.03.041.
[51] G.B. Scott, H.S. Williams, P.M. Marriott, The phagocytosis of colloidal particles of different sizes., Br. J. Exp. Pathol. 48 (1967) 411–416.
[52] B.D. Chithrani, A.A. Ghazani, W.C.W. Chan, Determining the Size and Shape Dependence of Gold Nanoparticle Uptake into Mammalian Cells, Nano Lett. 6 (2006) 662–668. doi:10.1021/nl052396o.
[53] T.S. Hauck, A.A. Ghazani, W.C.W. Chan, Assessing the Effect of Surface Chemistry on Gold Nanorod Uptake, Toxicity, and Gene Expression in Mammalian Cells, Small. 4 (2008) 153–159. doi:10.1002/smll.200700217.
[54] X. Huang, I.H. El-Sayed, W. Qian, M.A. El-Sayed, Cancer Cell Imaging and Photothermal Therapy in the Near-Infrared Region by Using Gold Nanorods, J. Am. Chem. Soc. 128 (2006) 2115–2120. doi:10.1021/ja057254a.
[55] K.-S. Lee, M.A. El-Sayed, Gold and Silver Nanoparticles in Sensing and Imaging: Sensitivity of Plasmon Response to Size, Shape, and Metal Composition, J. Phys. Chem. B. 110 (2006) 19220–19225. doi:10.1021/jp062536y.
[56] T.K. Sau, C.J. Murphy, Seeded High Yield Synthesis of Short Au Nanorods in Aqueous Solution, Langmuir. 20 (2004) 6414–6420. doi:10.1021/la049463z.
[57] A. Gole, C.J. Murphy, Polyelectrolyte-Coated Gold Nanorods: Synthesis, Characterization and Immobilization, Chem. Mater. 17 (2005) 1325–1330. doi:10.1021/cm048297d.

[58] B. Guo, J. Zhao, C. Wu, Y. Zheng, C. Ye, M. Huang, S. Wang, One-pot synthesis of polypyrrole nanoparticles with tunable photothermal conversion and drug loading capacity, Colloids Surf. B Biointerfaces. 177 (2019) 346–355. doi:10.1016/j.colsurfb.2019.02.016.
[59] X. Li, Y. Gong, X. Zhou, H. Jin, H. Yan, S. Wang, J. Liu, Facile synthesis of soybean phospholipid-encapsulated MoS2 nanosheets for efficient in vitro and in vivo photothermal regression of breast tumor, Int. J. Nanomedicine. 11 (2016) 1819–1833. doi:10.2147/IJN.S104198.
[60] Ž. Krpetić, F. Porta, E. Caneva, V. Dal Santo, G. Scarì, Phagocytosis of Biocompatible Gold Nanoparticles, Langmuir. 26 (2010) 14799–14805. doi:10.1021/la102758f.
[61] B.J. Nablo, T.-Y. Chen, M.H. Schoenfisch, Sol−Gel Derived Nitric-Oxide Releasing Materials that Reduce Bacterial Adhesion, J. Am. Chem. Soc. 123 (2001) 9712–9713. doi:10.1021/ja0165077.
[62] S. BarathManiKanth, K. Kalishwaralal, M. Sriram, S.R.K. Pandian, H. Youn, S. Eom, S. Gurunathan, Anti-oxidant effect of gold nanoparticles restrains hyperglycemic conditions in diabetic mice, J. Nanobiotechnology. 8 (2010) 16. doi:10.1186/1477-3155-8-16.
[63] B.P. Thornton, V. Větvicka, M. Pitman, R.C. Goldman, G.D. Ross, Analysis of the sugar specificity and molecular location of the beta-glucan-binding lectin site of complement receptor type 3 (CD11b/CD18), J. Immunol. Baltim. Md 1950. 156 (1996) 1235–1246.
[64] R. Shukla, V. Bansal, M. Chaudhary, A. Basu, R.R. Bhonde, M. Sastry, Biocompatibility of Gold Nanoparticles and Their Endocytotic Fate Inside the Cellular Compartment: A Microscopic Overview, Langmuir. 21 (2005) 10644–10654. doi:10.1021/la0513712.
[65] S.V. Tsoni, G.D. Brown, β-Glucans and Dectin-1, Ann. N. Y. Acad. Sci. 1143 (2008) 45–60. doi:10.1196/annals.1443.019.

Figure legends

Figure 1. (a) Molecular weight of β-D-glucan D1 measured by size exclusion chromatography - multi angle light scattering (SEC-MALS); (b) 1H Nuclear magnetic resonance (NMR) spectrum of D1. The Proton NMR spectra of the carbohydrate region of water insoluble particulate β-D-glucan in a mixed solvent (DMSO‑d6) at 80 °C.

Figure 2. Ultraviolet visible (UV-Vis) absorption spectra of the aqueous solutions of (a) AuNPs (50 nM) reduced by citrate; (b) β-D-glucans (1 mg/mL); (c) β-D-gluc+AuNP10; and (d) β-D-gluc+AuNP50. The inset image is a photo of the corresponding mixture.

Figure 3. Micrographs of AuNPs and β-D-glucans by transmission electron microscopy. (a) β-D-glucans solubilized in water (1 mg/mL); (b) AuNPs (50nM) reduced by citrate at 90 ^{0}C; (c) β-D-gluc+AuNP10 system that contains AuNPs (10nM) reduced by β-D-glucans (1 mg/mL) at 90 ^{0}C; (d) β-D-gluc+AuNP50 system that contains AuNPs (50nM) reduced by β-D-glucans (1 mg/mL) at 90 ^{0}C. The inset images are a magnification of the AuNPs reduced on the outer surface of β-D-glucans.

Figure 4. Effect of β-D-glucans, β-D-gluc+AuNP10, β-D-gluc+AuNP50, AuNP10, and AuNP50 at 24 h on the viability of splenocytes. Viability was assessed at the end of 24 h by measuring resazurin fluorescence. Data are shown as mean ± SD; statistical differences ($P < 0.05$) were calculated, and different letters in the block denote significant difference.

Figure 5. (a) Phagocytic ability and (b) reactive oxygen species (ROS) production by DHR123 of splenocytes stimulated with β-D-glucans, β-D-gluc+AuNP10, β-D-gluc+AuNP50, AuNP10, and AuNP50 at 24 h. Data are shown as mean ± SD; statistical differences ($P < 0.05$) were calculated, and different letters in the block denote significant difference.

Figure 6. (a) Nitric oxide production and (b) peroxidase activity of splenocytes stimulated with β-D-glucans, β-D-gluc+AuNP10, β-D-gluc+AuNP50, AuNP10, and AuNP50 at 24 h. Data are shown as mean ± SD; statistical differences ($P < 0.05$) were calculated, and different letters in the block denote significant difference.

Figure 7. (a) Superoxide dismutase and (b) catalase activities of splenocytes stimulated with β-D-glucans, β-D-gluc+AuNP10, β-D-gluc+AuNP50, AuNP10, AuNP50 at 24 h. Data are shown as

mean ± SD; statistical differences ($P < 0.05$) were calculated, and different letters in the block denote significant difference.

Figure 8. Quantitative reverse transcription polymerase chain reaction (RT-qPCR) of cell mediated immune marker genes in splenocytes of stimulated mice after 24 h. The mRNA level of each gene was normalized to that of β-actin. Mean and SD (of 6 pools). Data are shown as mean ± S.D. fold increase relative to control. Different letters denote significant difference between treated groups ($P < 0.05$).

Figure 9. Representative scanning electron microscopy (SEM) images of interaction between spleen leukocytes and β-D-glucan, AuNP10 and AuNP50 after 24 h of exposure; (a) spleen leukocytes, (b) leukocytes + β-D-glucan, (c) leukocytes + AuNP10, (d) leukocytes + β-D-glucan + AuNP10, (e) leukocytes + AuNP50, (f) leukocytes + β-D-glucan + AuNP50. L: Leukocytes. G: β-D-glucan. Blue arrow: AuNP10. Red arrow: AuNP50. Yellow arrow: Apoptosis. (For interpretation of the references to color in this figure legend, the reader is referred to the Web version of this article.)

Tables

Table I. Sequences of the primers used in this study analyzing the effect of AuNPs, β-D-glucans, and β-D-gluc+AuNPs in mouse leukocytes.

Table II. Dynamic light scattering (DLS) measurements that show pH, ζ-potential and hydrodynamic radius of AuNPs, β-D-glucans, and β-D-gluc+AuNPs systems.

Compliance with ethical standards

Conflict of interest

All authors declare that they have no conflicts of interest.

Ethical approval

All applicable international, national, and/or institutional guidelines for the care and use of animals were followed.

Tables

Table I. Sequences of the primers used in this study

Gen	Abbreviation	Length of product	Accesion No.	Primer sequences (5'-3')
Dectin-1	Dectin-1	192	NM_001309637.1	GACTTCAGCACTCAAGACATCC CCCATGCATGATCCAATTAG
Nuclear factor kappa-light-chain-enhancer of activated B cells	NF-κβ	190	NM_008689.2	CTATGACCTGGACGACTCTTG CCTCGTGTCTTCTGTCAGC
Interleukin-1β	IL-1β	182	NM_008361.4	GCAGGCAGTATCACTCATTG GTCTAATGGGAACGTCACAC
Tumor Necrosis Factor-α	TNF-α	156	NM_013693.3	ACAGAAAGCATGATCCGC CCCGAAGTTCAGTAGACAGAAG

Table II. DLS measurements that shows the pH, ζ-potential and hydrodynamic radius of AuNPs, β-D-glucans, and β-D-gluc+AuNps systems.

System	pH	ζ-potential (mV)	Hydrodynamic radius (nm)
AuNps	4	-24.06 ± 3.2	25.61 ± 0.6
β-D-glucan	5	4.47 ± 0.6	4247.66 ± 509.76
β-D-gluc+AuNp10	5	6.75 ± 1.4	5820.00 ± 348.31
β-D-gluc+AuNp50	5	-1.01 ± 0.2	5192.66 ± 341.08

Highlights

- This work reports a novel methodology to produce metallic nanoparticles or 1D nanostructures by using β-D-glucans isolated from a yeast *Yarrowia lypolitica* D1.

- β-D-gluc+AuNP10 and β-D-gluc+AuNP50 caused an important cytotoxicity in mice spleen leukocytes, while bare β-D-glucan or AuNPs alone, did not.

- The β-D-gluc+AuNPs systems may not be candidates for the formulation of immunostimulants or nanocarriers for biomedical applications.

a)

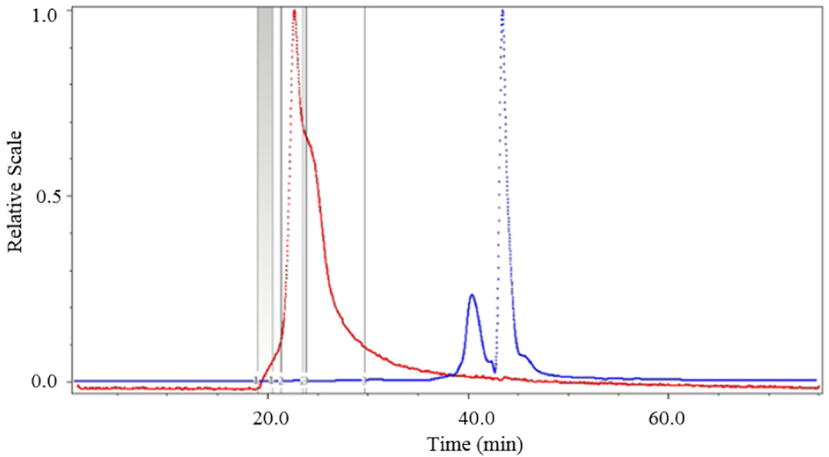
1.0
0.5
0.0
Relative Scale
20.0
40.0
60.0
Time (min)

b)

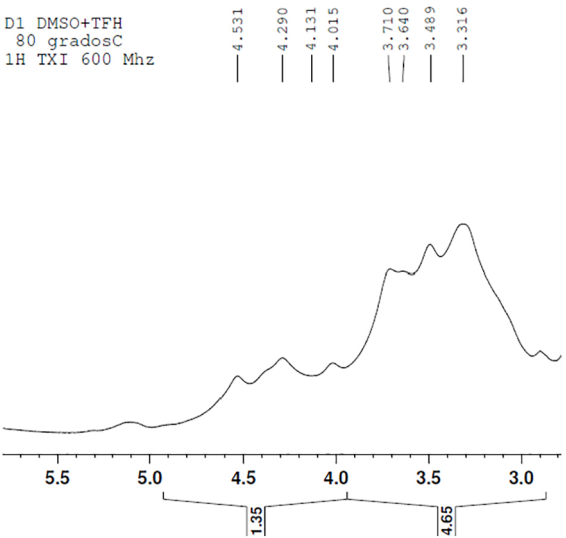
D1 DMSO+TFH
80 gradosC
1H TXI 600 Mhz
4.531
4.290
4.131
4.015
3.710
3.640
3.489
3.316
5.5
5.0
4.5
4.0
3.5
3.0
1.35
4.65

Figure 1

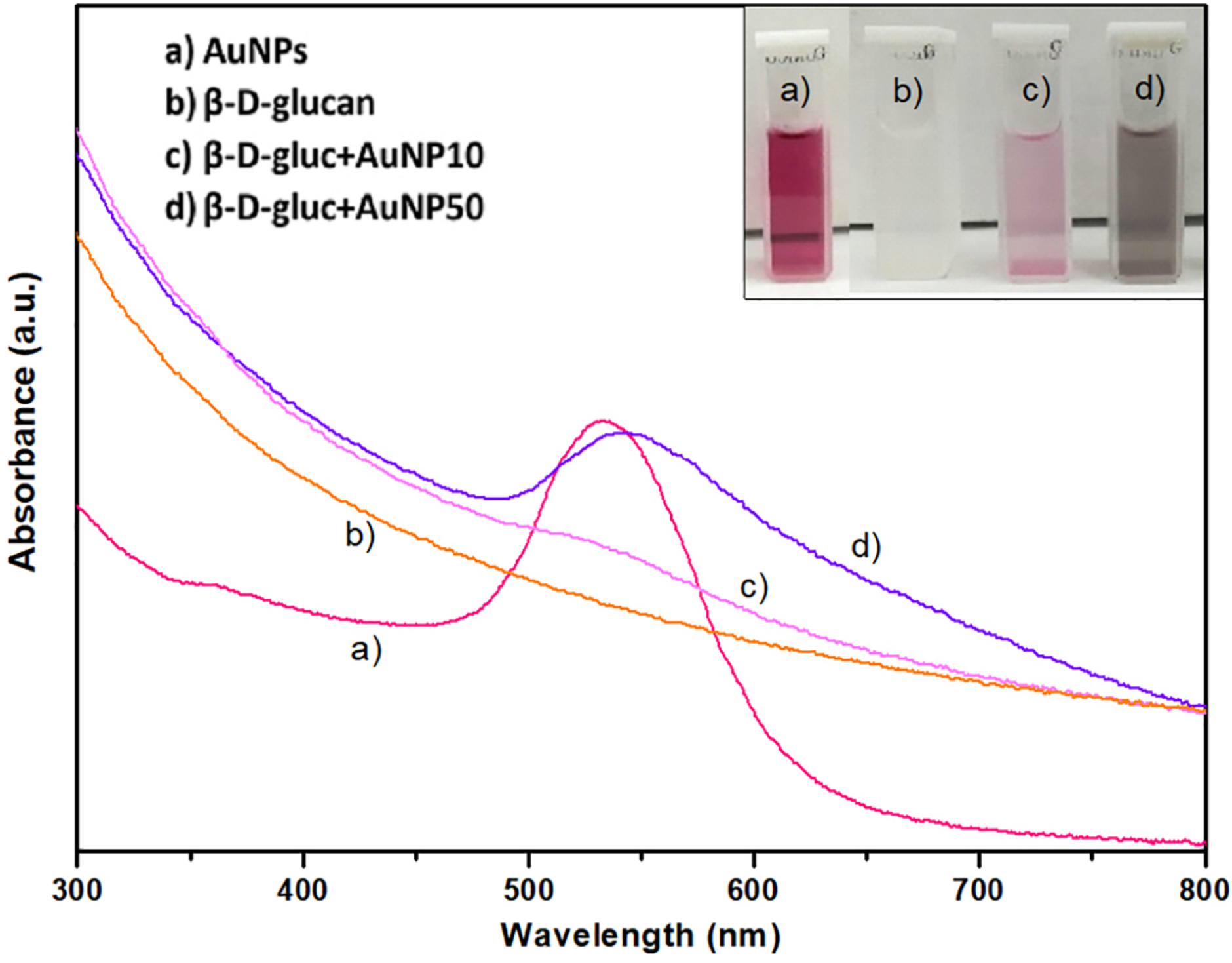
a) AuNPs
b) β-D-glucan
c) β-D-gluc+AuNP10
d) β-D-gluc+AuNP50
a)
b)
c)
d)
Absorbance (a.u.)
300
400
500
600
700
800
Wavelength (nm)

Figure 2

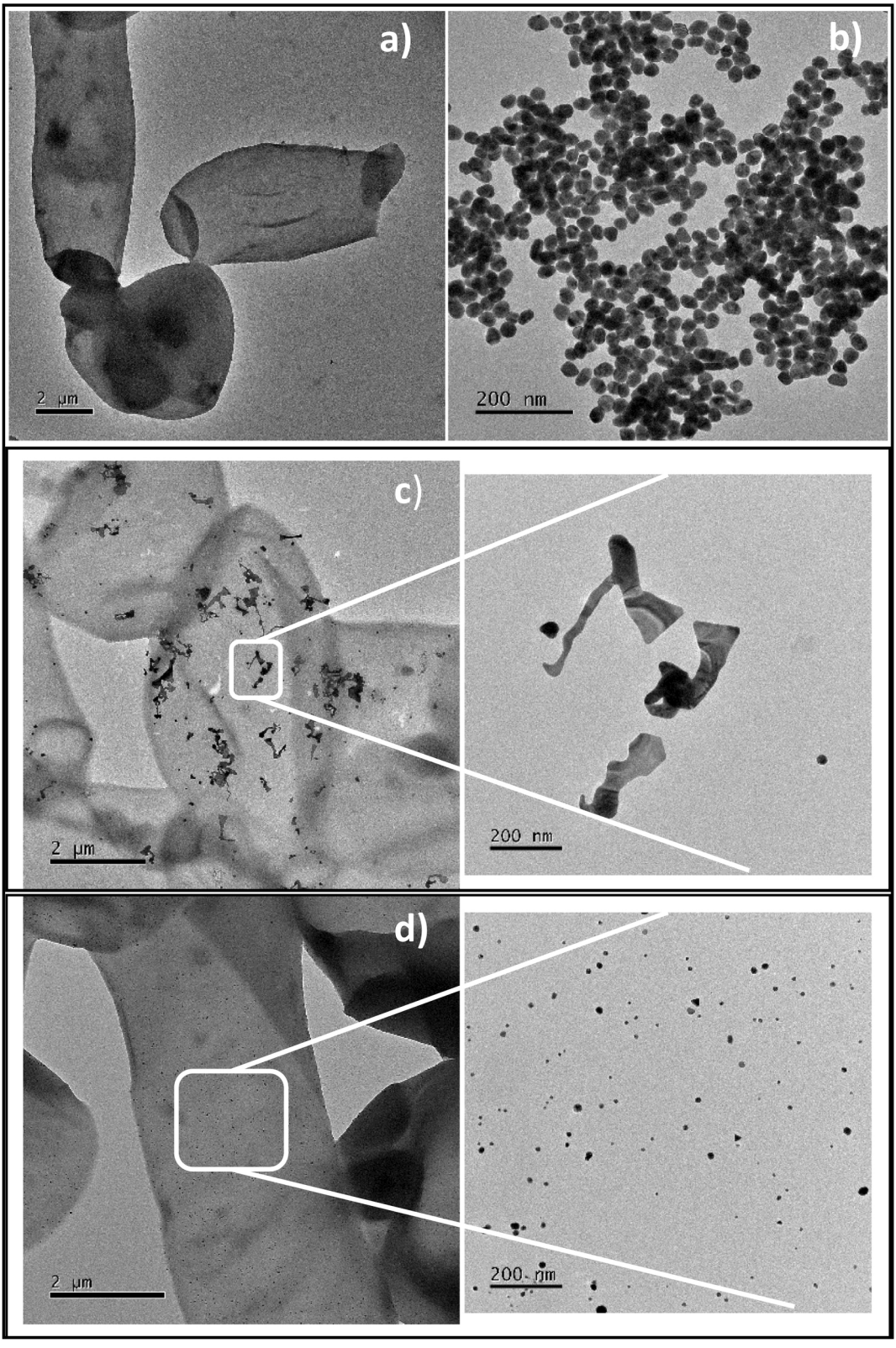

Figure 3

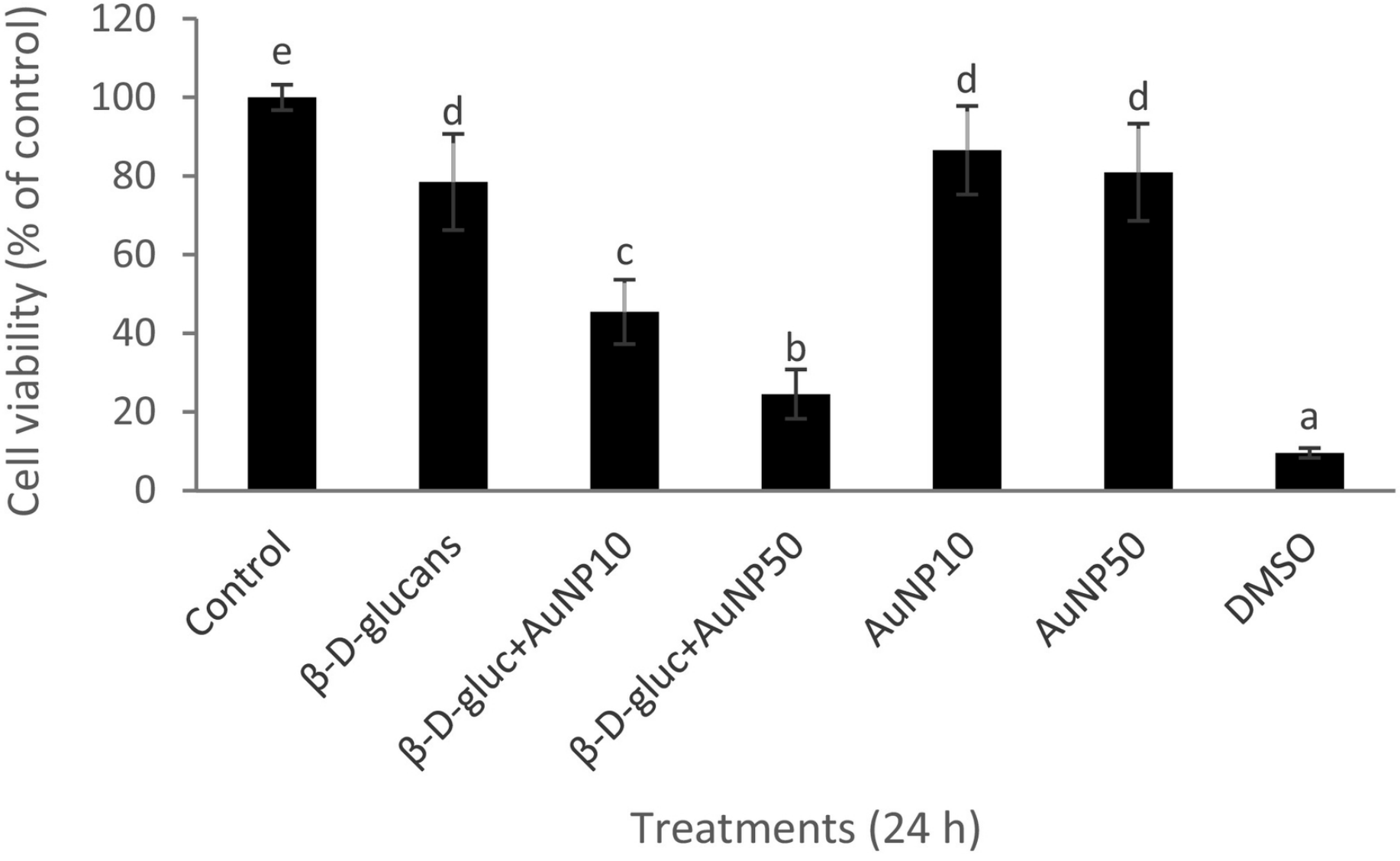
Cell viability (% of control)
120
100
80
60
40
20
0
e
d
c
b
d
d
a
Control
β-D-glucans
β-D-gluc+AuNP10
β-D-gluc+AuNP50
AuNP10
AuNP50
DMSO
Treatments (24 h)

Figure 4

a

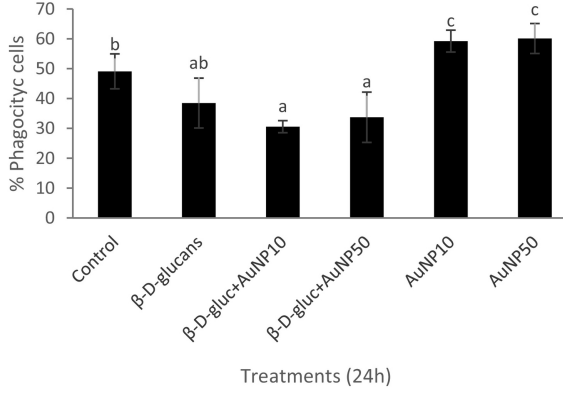
% Phagocityc cells
70
60
50
40
30
20
10
0
b
ab
a
a
c
c
Control
β-D-glucans
β-D-gluc+AuNP10
β-D-gluc+AuNP50
AuNP10
AuNP50
Treatments (24h)

b

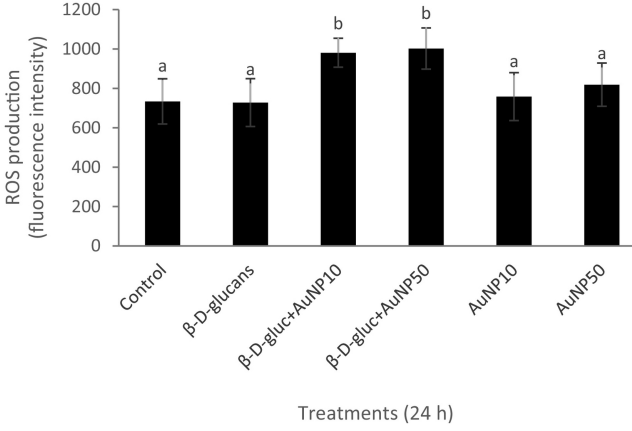
ROS production
(fluorescence intensity)
1200
1000
800
600
400
200
0
a
a
b
b
a
a
Control
β-D-glucans
β-D-gluc+AuNP10
β-D-gluc+AuNP50
AuNP10
AuNP50
Treatments (24 h)

Figure 5

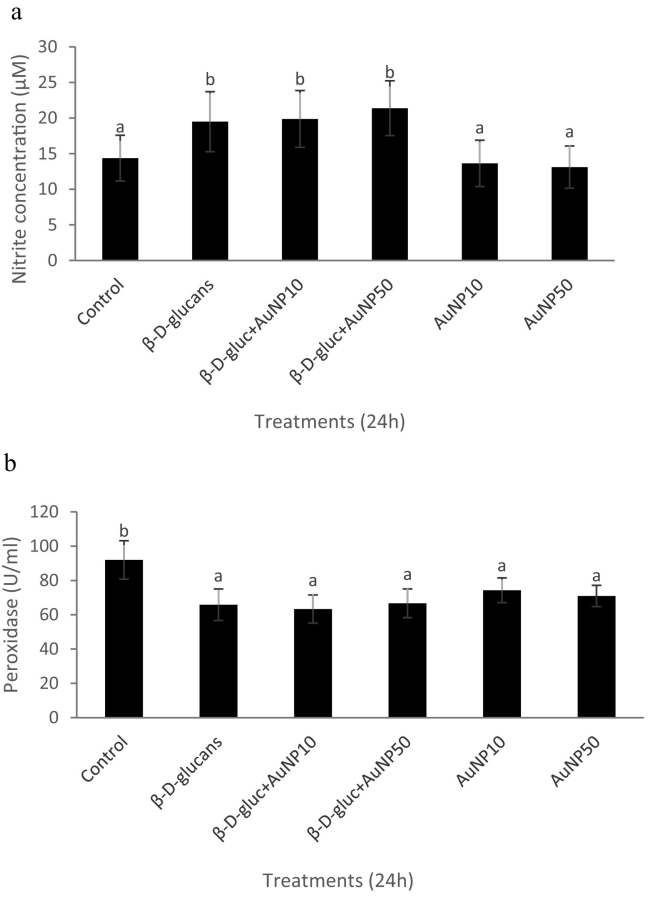
a
Nitrite concentration (µM)
30
25
20
15
10
5
0
a
b
b
b
a
a
Control
β-D-glucans
β-D-gluc+AuNP10
β-D-gluc+AuNP50
AuNP10
AuNP50
Treatments (24h)
b
Peroxidase (U/ml)
120
100
80
60
40
20
0
b
a
a
a
a
a
Control
β-D-glucans
β-D-gluc+AuNP10
β-D-gluc+AuNP50
AuNP10
AuNP50
Treatments (24h)

Figure 6

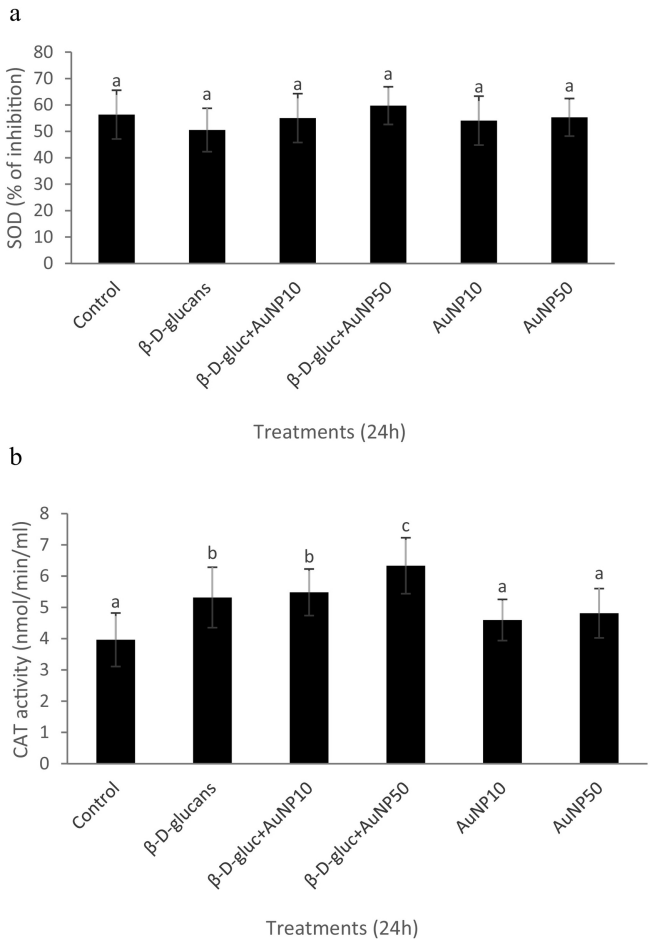
a
SOD (% of inhibition)
80
70
60
50
40
30
20
10
0
a
a
a
a
a
a
Control
β-D-glucans
β-D-gluc+AuNP10
β-D-gluc+AuNP50
AuNP10
AuNP50
Treatments (24h)
b
CAT activity (nmol/min/ml)
8
7
6
5
4
3
2
1
0
a
b
b
c
a
a
Control
β-D-glucans
β-D-gluc+AuNP10
β-D-gluc+AuNP50
AuNP10
AuNP50
Treatments (24h)

Figure 7

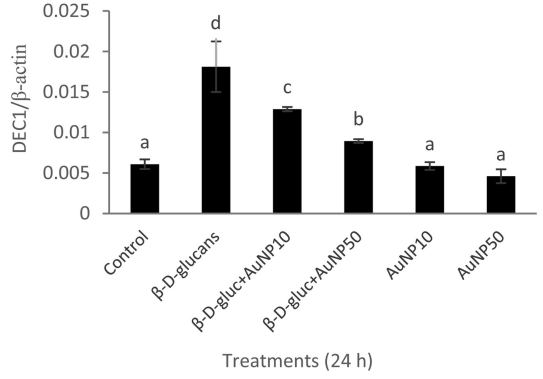
DEC1/β-actin
0.025
0.02
0.015
0.01
0.005
0
a
d
c
b
a
a
Control
β-D-glucans
β-D-gluc+AuNP10
β-D-gluc+AuNP50
AuNP10
AuNP50
Treatments (24 h)

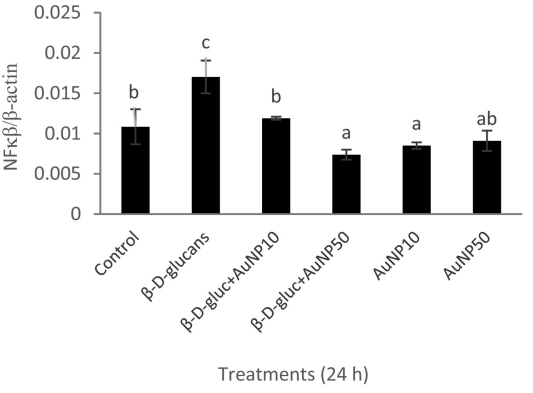
NFκβ/β-actin
0.025
0.02
0.015
0.01
0.005
0
b
c
b
a
a
ab
Control
β-D-glucans
β-D-gluc+AuNP10
β-D-gluc+AuNP50
AuNP10
AuNP50
Treatments (24 h)

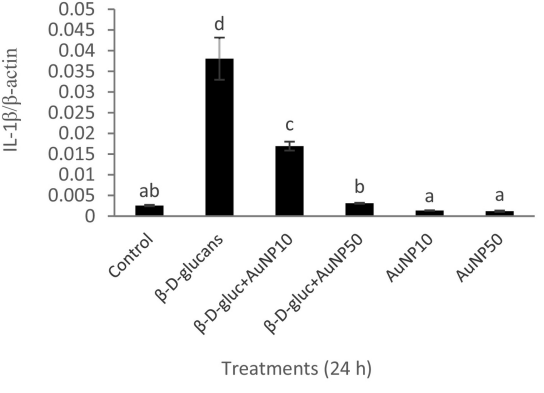
IL-1β/β-actin
0.05
0.045
0.04
0.035
0.03
0.025
0.02
0.015
0.01
0.005
0
ab
d
c
b
a
a
Control
β-D-glucans
β-D-gluc+AuNP10
β-D-gluc+AuNP50
AuNP10
AuNP50
Treatments (24 h)

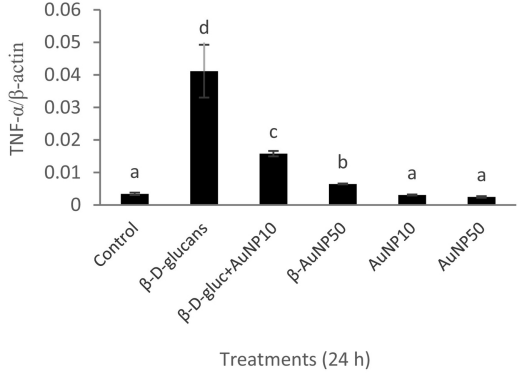
TNF-α/β-actin
0.06
0.05
0.04
0.03
0.02
0.01
0
a
d
c
b
a
a
Control
β-D-glucans
β-D-gluc+AuNP10
β-AuNP50
AuNP10
AuNP50
Treatments (24 h)

Figure 8

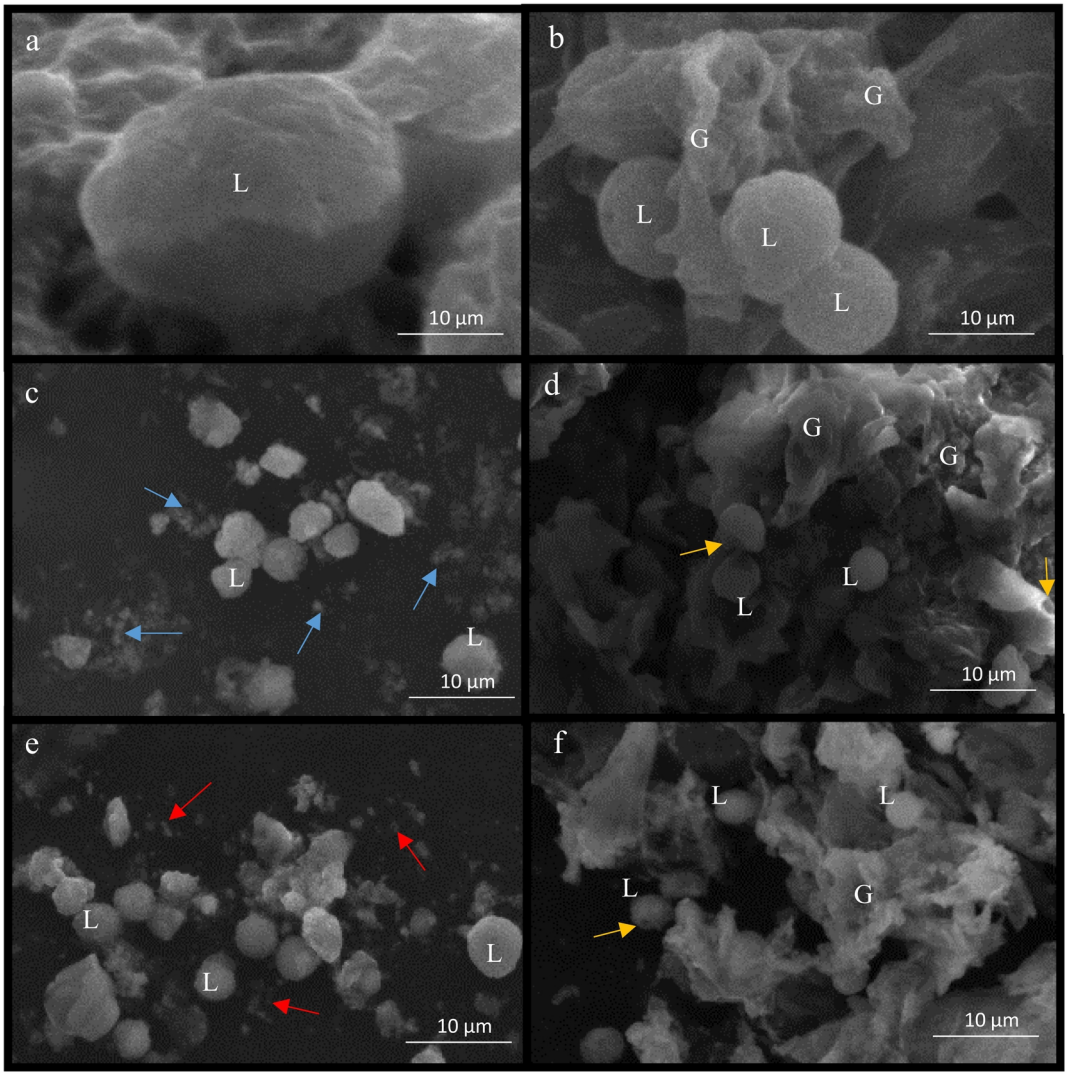

Figure 9